Applied Clay Science 186 (2020) 105439

Contents lists available at ScienceDirect

Applied Clay Science

journal homepage: www.elsevier.com/locate/clay

Research paper

Methane hydrate formation in the stacking of kaolinite particles with different surface contacts as nanoreactors: A molecular dynamics simulation study

Yun Li[a,b], Meng Chen[a,b], Hongzhe Song[a,b], Peng Yuan[a,b,*], Dong Liu[a,b], Baifa Zhang[a,b], Hongling Bu[a,b]

[a] CAS Key Laboratory of Mineralogy and Metallogeny, Guangdong Provincial Key Laboratory of Mineral Physics and Materials, Guangzhou Institute of Geochemistry, Institutions of Earth Science, Chinese Academy of Sciences (CAS), Guangzhou 510640, China
[b] University of Chinese Academy of Sciences, Beijing 100049, China

ARTICLE INFO

Keywords:
CH_4 hydrate
Kaolinite
Siloxane surface
Hydroxyl surface
Molecular simulations

ABSTRACT

The heterogeneous nucleation behaviors of methane (CH_4) hydrate in the presence of kaolinite (Kaol) were studied, and nucleation was found to be strongly affected by the surface contacts of Kaol particles. Molecular dynamics simulations were performed to investigate CH_4 hydrate formation in Kaol particles with different surface contacts, such as silica-alumina face, alumina-alumina face, and silica-silica face. The results revealed two nucleation events, one in the bulk-like solution and the other near the siloxane surface of the Kaol. The crystal growth of CH_4 hydrate tended to occur away from the Kaol surface. The silicon-oxygen rings of the siloxane surface served as a plane of the cage, thereby forming a semi-cage arrangement in which the CH_4 molecules appeared to have the ability to stabilize the arrangement of water structures. However, strong hydrogen bond interactions made it difficult for CH_4 molecules to form clathrate-like structures on the hydroxyl surface. These results indicate that Kaol particles with a siloxane surface promoted CH_4 hydrate nucleation and growth but that Kaol particles with a hydroxyl surface were unable to do so. Thus, the surface properties and surface contacts of Kaol particles were found to involve in the formation of aggregates in natural sediments, which shows that they are crucial for nucleation, distribution, and crystallinity of CH_4 hydrate.

1. Introduction

Gas hydrate is an ice-like solid substance composed of water (H_2O) and gas molecules (e.g., methane [CH_4], carbon dioxide [CO_2], or ethane) (Sloan, 2003; Sloan and Koh, 2007). H_2O molecules form hydrogen bonds (HB) to establish a polyhedral cage structure that encapsulates gas molecules at high pressures and in low-temperature environments (Sloan and Koh, 2007). Three types of hydrate structures are formed naturally, depending principally on the size of the gas molecule, cubic structure I (sI), cubic structure II (sII), and hexagonal structure H (sH) (Sloan, 2003; Wei et al., 2018). In the case of CH_4 hydrate, type sI is formed with six $5^{12}6^2$ (12 pentagons and 2 hexagons) and two 5^{12} cages. CH_4 hydrate is abundant in permafrost and marine sediments, and the amount of energy stored in CH_4 hydrate is estimated to be twice that embodied in conventional fossil fuel resources (Sloan and Koh, 2007). Given the current emphasis on the development of clean energy supplies to reduce global environmental pollution problems (Sloan, 2003; Zatsepina and Pooladi-Darvish, 2011; Boswell et al., 2012), studies of the nucleation and growth mechanism of CH_4 hydrate have increased in recent decades.

The examination of gas-hydrate formation kinetics (Lee et al., 2002; Wang et al., 2015) and phase-equilibrium conditions (Kyung et al., 2014; Kim et al., 2015) in laboratory experiments has suggested that hydrate nucleation and growth is a phenomenon that may be used to evaluate the gas storage capacity and the stability of stored gas hydrate in geological formations with long-term stability. Accordingly, experimental studies have demonstrated that natural sediments significantly affect the hydrate formation process by altering nucleation time and formation rates (Lee et al., 2013; Kyung et al., 2015) and have suggested that hydrate formation kinetics depend significantly on the type (Lamorena and Lee, 2008, 2009) and surface properties (Lamorena and Lee, 2008, 2009; Park et al., 2014) of the minerals in the natural

* Corresponding author at: CAS Key Laboratory of Mineralogy and Metallogeny, Guangzhou Institute of Geochemistry, Chinese Academy of Sciences (CAS), Wushan, Guangzhou, 510640, China.
E-mail address: yuanpeng@gig.ac.cn (P. Yuan).

https://doi.org/10.1016/j.clay.2020.105439
Received 18 November 2019; Received in revised form 3 January 2020; Accepted 5 January 2020
Available online 09 January 2020
0169-1317/

sediment (i.e., surface charge, specific surface area, and chemical species on the mineral surface). In particular, the most abundant clay minerals (i.e., smectite, illite, kaolinite, and chlorite) are representative geochemical components in natural sediments (Guggenheim and van Groos, 2003; Uchida et al., 2004; Seo et al., 2009; Yeon et al., 2011; Kim et al., 2015), so further investigation is warranted to evaluate the effects of clay minerals on the formation of natural gas hydrate. Some studies have demonstrated that the clay mineral surface provides nucleation sites that facilitate hydrate crystallization, resulting in rapid hydrate formation kinetics (Park and Sposito, 2003; Lamorena and Lee, 2009). In addition, the clay mineral surface was found to extend the lifetime of cage structures. For example, a phase-equilibrium experiment of CO_2 hydrate in clay mineral suspensions was conducted by Park et al., who demonstrated that the presence of montmorillonite significantly affected CO_2 hydrate stability due to the electrostatic attraction between cations and H_2O molecules (Park et al., 2014). These studies suggested that identifying the reaction mechanism between gas hydrate and clay minerals was crucial to understand the formation, distribution, and stability of gas hydrate in geologic sediments.

Kaolinite (Kaol) is one of the most widely occurring clay minerals in the marine sediments in which oil and gas resources reside (Özen et al., 2015; Zhang et al., 2016). Many studies have found that the clay minerals in gas hydrate bearing sediments contain a relatively high content of Kaol; indeed, Kaol accounts for 17.3% in Ulleung Basin sediment (Lamorena et al., 2011), and 16% to 18% in the southwestern region of the South China Sea (Schroeder et al., 2015). Kaol is a 1:1 dioctahedral clay mineral in which each layer contains a tetrahedral silica sheet and an octahedral alumina sheet. This is distinct from typical 2:1 dioctahedral clay minerals, which have one octahedral alumina sheet between two opposing tetrahedral silica sheets. The adjacent octahedral and tetrahedral sheets of Kaol are bound by HB, and H_2O molecules cannot enter the interlayer (Bergaya et al., 2013; Brigatti et al., 2013). In addition, the octahedral and tetrahedral surfaces of Kaol exhibit different degrees of affinity for H_2O: the octahedral surface forms strong HB with H_2O molecules, whereas the tetrahedral surface forms only weak HB with H_2O molecules. Thus, the octahedral and tetrahedral surfaces display hydrophilic and hydrophobic properties, respectively (Tunega et al., 2002, 2004). These unique structural properties and surface chemistries of Kaol suggest that Kaol particles generally adopt random–layered stack behavior in natural environments (Johnson et al., 1998, 2000). Studies have determined that (Żbik et al., 2008; Żbik and Frost, 2009; Gupta et al., 2011), the marine sediment environmental factors (such as pH and the types of inorganic salt ions present) are likely to influence the contact behaviors of Kaol particles, generating various surface contacts, such as silica-alumina face, silica-silica face, alumina-alumina face, edge-silica face, edge-alumina face, and edge-edge. These different surface contacts of Kaol particles constitute different types of nanoreactors, in which the properties of the inner surface are dependent on the type of surface contact with which it is involved. It has been shown that the chemical properties of a solid surface alter the formation kinetics of CH_4 hydrate, due to the different affinities possible between the solid surface and CH_4 and H_2O molecules (Nguyen et al., 2017; Defever and Sarupria, 2018). It follows that the abovementioned nanoreactors that result from the stacking of Kaol particles may substantially affect the formation of CH_4 hydrate. This raises a key question: how does the microstructure of Kaol (i.e., its different surface contacts) influence the nucleation and growth mechanism of CH_4 hydrate? Unfortunately, it would be technically prohibitive to answer this question by using commonly used phase equilibrium experiments, because it is technically challenging to investigate the formation mechanism at the molecular scale of CH_4 hydrate in Kaol with different surface contacts. However, molecular dynamics (MD) simulations are a powerful tool in such conditions because they enable the investigation of CH_4 hydrate formation in the presence of clay minerals at the molecular level (Cygan et al., 2004a; Martos-Villa et al., 2014a, 2014b; Yan et al., 2016; Ji et al., 2017; Cox et al., 2018). Additionally, several MD simulation works relevant to pure CH_4 hydrate nucleation and crystal growth have been reported. For example, Walsh et al. reported the nucleation of CH_4 hydrate at the interface between CH_4 vapor and liquid H_2O using MD simulation. They observed the types of cages formed during the nucleation process and calculated the nucleation rate based on the induction time. The nucleation rate increased with the increasing CH_4 concentration under different thermodynamic conditions (Walsh et al., 2009, 2011). Liang et al. studied the crystal growth of CH_4 hydrate at the interface between solid hydrate phase and liquid H_2O. They showed that the $5^{12}6^3$ cages were formed as intermediates during CH_4 hydrate formation (Liang and Kusalik, 2010). Thus, MD simulation can be used to simulate and even reproduce the formation process of CH_4 hydrate, thereby affording data that are experimentally inaccessible.

In this work, MD simulations were performed to investigate the arrangement of CH_4 and H_2O molecules in Kaol nanoreactors with different surface contacts during CH_4 hydrate formation. To evaluate the role of the Kaol surface in CH_4 hydrate formation at an atomic and molecular level, three types of surface contact for Kaol particles were simulated: silica-alumina face (Fsa), alumina-alumina face (Faa), and silica-silica face (Fss). The formation mechanisms of the surface contacts of Kaol in geologic sediments and the nucleation and growth behavior of CH_4 hydrate were proposed based on the simulation results, and the implications of these results are discussed.

2. Computation methods

2.1. Simulation models

Kaol ($Al_4[Si_4O_{10}](OH)_8$) is a typical 1:1 clay mineral that comprises a tetrahedral silica sheet and an octahedral alumina sheet. The two sheets are closely bonded, as they share a plane of oxygen atoms, and the repeating layers are stacked and connected by HB (Bergaya et al., 2013; Bish, 1993). In this work, the simulated Kaol model consisted of two platelets with 48 unit cells: six in the x dimension, four in the y dimension, and two in the z dimension, forming a patch of lx = 3.092 and ly = 3.577 nm. Two platelets of the Kaol sheet were oriented in the [001] direction, with a bulk solution model inserted between. This bulk solution model for the CH_4–H_2O phase was a randomly distributed set of 140 CH_4 and 1610 H_2O molecules with a thickness of approximately 5 nm. The molar fraction of CH_4 in this simulation satisfied the condition that the CH_4 molecules would remain uniformly distributed in the liquid H_2O without phase separation (Jiménez-Ángeles and Firoozabadi, 2014; Bhattacharjee et al., 2016). The total height of the simulation model was approximately 8 nm. Therefore, three types of Kaol models (i.e., Fsa, Faa, and Fss) and the bulk solution model (MH) were built. The initial configurations of these models are shown in Fig. 1.

2.2. Simulation details

The ClayFF force field was used to describe Kaol (Table S1) (Cygan et al., 2004b). The TIP4P-ice model was used for H_2O, and the settle algorithm was used to constrain the rigid geometry of the H_2O molecules (Abascal et al., 2005). The OPLS-AA model was used for CH_4 (Jorgensen et al., 1984). The combination of a force field and models has been shown to work well in previous studies (Ji et al., 2017; Wu et al., 2018). The Lorentz-Berthelot mixing rules were applied to calculate the Lennard-Jones potentials between atoms (Allen and Tildesley, 2017). Short-range non-bonded interactions were truncated at 1.25 nm. The particle-mesh Ewald method was used to calculate the long-range electrostatic interactions with a Fourier spacing of 0.12 nm (Darden et al., 1993). The equations of motion were integrated with the leapfrog algorithm using a time-step of 1.0 fs (Van Gunsteren and Berendsen, 1988). These simulations were performed in orthorhombic boxes, and periodic boundary conditions were imposed on the

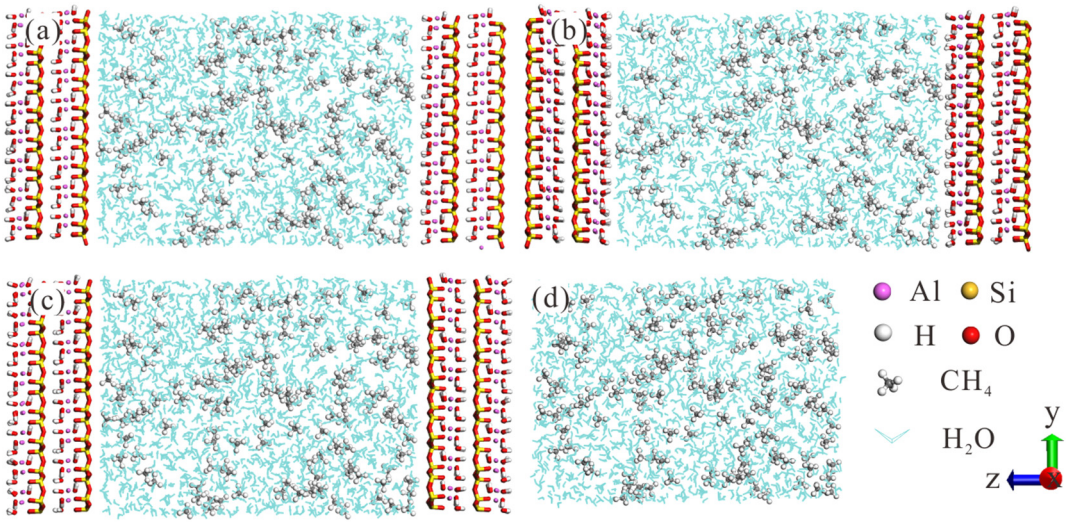

Fig. 1. Initial configurations of the simulation models: (a) Fsa; (b) Faa; (c) Fss; (d) MH.

molecular structures (Makov and Payne, 1995). All simulations were performed with the GROMACS 5.1.2 package (Hess et al., 2008). The simulation temperature and pressure were 250 K and 50 MPa, respectively, which were chosen to ensure that sufficient a driving force existed to enable the growth kinetics of CH_4 hydrate to be obtained from the simulation (Vatamanu and Kusalik, 2006; Walsh et al., 2009; Jiménez-Ángeles and Firoozabadi, 2018). In each MD simulation, energy minimization was performed with a steepest-descent algorithm to relax the initial configuration. After energy minimization, short equilibration was conducted via a 2-ns isothermal-isobaric ensemble (*NpT*) simulation. Finally, the equilibrated configuration was processed in an *NpT* simulation for 1 μs, with the temperature-controlled by a Nosé-Hoover thermostat (Evans and Holian, 1985) with a time-constant of 1 p and the pressure-controlled by a Parrinello-Rahman barostat (Parrinello and Rahman, 1981) with a time-constant of 4 ps. Notably, only the z dimension is scaled in *NpT* simulations.

2.3. Data analysis

A tetrahedral order parameter (F_3) (Baez and Clancy, 1994) and a four-body order parameter (F_4) (Rodger et al., 1996; Moon et al., 2007) were applied to analyze the order of water molecules, and these were defined as follows (Eqs. (1) and (2)):

$$F_3 = \left\langle \sum_{j=1}^{n_i-1} \sum_{k=j+1}^{n_i} \left(|\cos\theta_{jik}|\ \cos\theta_{jik} + \cos^2(109.47°)\right)^2 \right\rangle \quad (1)$$

where θ_{jik} denotes the angle between the specified oxygen i_{th} atom and the other two oxygen (i.e., j_{th} and k_{th}) atoms within a distance of 0.35 nm around the i_{th} atoms, and n_i denotes the number of oxygen atoms. Average $\langle\ldots\rangle$ were computed over all H_2O molecules. The average values of the F_3 parameter remained approximately equal to 0.1 for liquid water and 0.01 for solid water (including CH_4 hydrate and ice).

$$F_4 = \frac{1}{n} \sum_{i=1}^{n} \cos 3\phi_i \quad (2)$$

where ϕ_i denotes the dihedral angle between the oxygen atoms of two adjacent molecules and the outermost hydrogen atoms, and n indicates the number of the oxygen atom pairs of H_2O molecules within 0.35 nm. The average values of F_4 were -0.04, -0.4, and 0.7 for H_2O, ice, and CH_4 hydrate, respectively.

The cage analysis algorithm that was used was similar to that proposed by Jacobson et al. (2009). Thus, the H_2O structure was identified by searching for the oxygen atoms within 0.61 nm of the central CH_4 molecules. The topological structure of the ring was determined by the connectivity of the H_2O molecules. Two oxygen atoms were deemed to be connected if they were separated by < 0.35 nm. A search was then made for all pentagonal and hexagonal rings that could possibly form from the connected oxygen atoms. Oxygen atoms were taken as the vertices to identify the 5^{12}, $5^{12}6^2$, $5^{12}6^3$, and $5^{12}6^4$ cages (Jiménez-Ángeles and Firoozabadi, 2014, 2015).

3. Results and discussion

3.1. Order parameter and hydrate cages analysis

3.1.1. Order parameter of H_2O molecules during the CH_4 hydrate formation

The order parameter of H_2O molecules can be used to identify the tendency of CH_4 hydrate formation. The hydrate phase and liquid phase were distinguished by order parameters from the simulation trajectory. Meanwhile, a decrease in the potential energy was also observed (Fig. S1). Fig. 2a and b show the evolution of F_3 and F_4, respectively, in different simulation models (averaged over all H_2O molecules). In a fully occupied sI of CH_4 hydrate, the CH_4/H_2O ratio is 1:5.75 (Sloan, 2003; Sloan and Koh, 2007), and the values of F_3 and F_4 are 0.01 and 0.7, respectively. In this work, the CH_4/H_2O ratio was 1:11.5, and this was interpreted to indicate that H_2O molecules cannot be completely converted into CH_4 hydrates; as a result, F_3 and F_4 also cannot reach the respective values of 0.01 and 0.7. The decrease in F_3 and the increase in F_4 with increasing simulation time indicated that nucleation and growth of CH_4 hydrate were occurring. It also indicated the molecular transformation of H_2O from a disordered state (liquid phase) to an ordered state (hydrate phase). The equilibrium values of F_3 and F_4 were between those of liquid H_2O and CH_4 hydrate, indicating that some H_2O molecules were also present in the liquid phase. During the first half of the simulation time (from 0 to 500 ns), a large number of CH_4 molecules were used to form CH_4 hydrate, and a small number of CH_4 molecules were used for the continued growth of CH_4 hydrate. Therefore, the fluctuation range of F_3 and F_4 was relatively small and reached a steady value during the second half of the simulation (from 500 to 1000 ns), which indicated that a large number of CH_4 hydrate cages had been formed. The trend of F_3 and F_4 can generally be used to assess the propensity of a model to form CH_4 hydrate, and thus the lower value F_3 in the Fss model showed that this model had a slightly higher propensity to form CH_4 hydrate than the Faa model. This result indicated that it was favorable to form better tetrahedral arrangement of H_2O molecules in the Fss model.

To further investigate the arrangement of H_2O molecules at the Kaol-H_2O interface, the order of the local H_2O structure on the Kaol

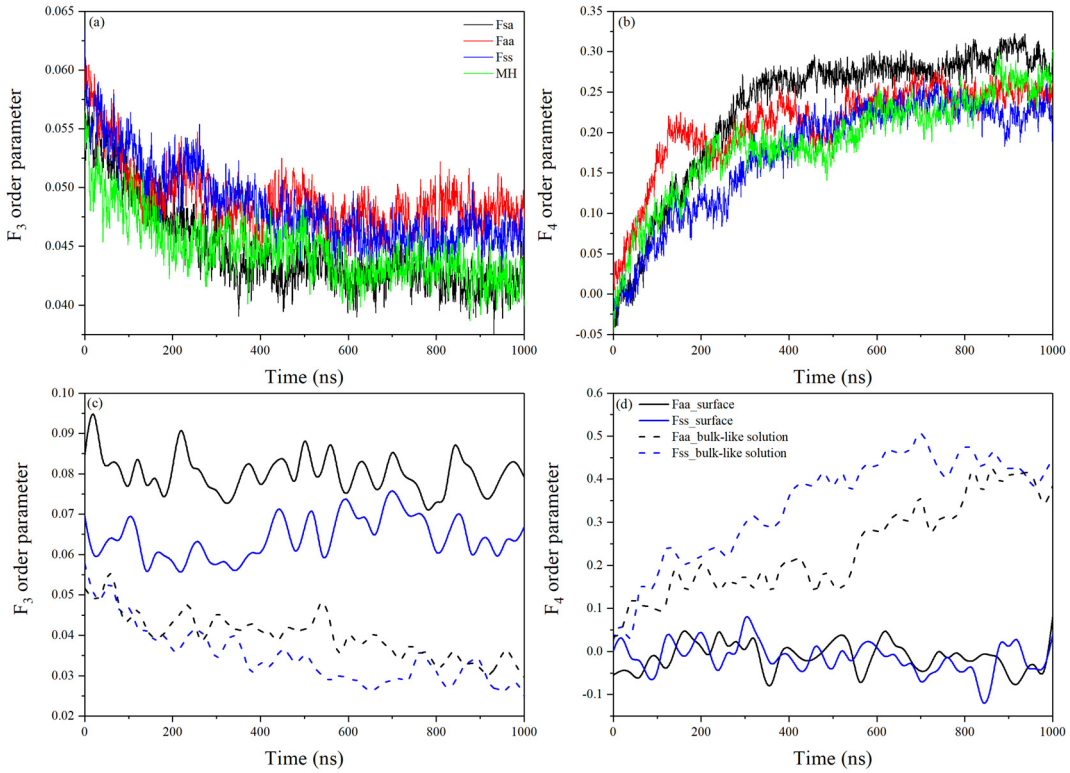

Fig. 2. Evolution of F_3 and F_4 in different simulation models.

surface (the first H_2O layer, < 1.8 nm) and the bulk-like solution (3.25 to 3.75 nm) were also examined (Fig. 2c and d). The slight difference in the equilibrium value of the F_3 and F_4 for different models might be due to the different effects of siloxane and hydroxyl surfaces on CH_4 hydrate formation. The values of F_3 and F_4 in the bulk-like solution were reasonably close to the average values of the hydrate crystal after CH_4 hydrate formation, which indicated that CH_4 hydrate formation was more favorable in the bulk-like solution than on the Kaol surface. The F_4 values indicate that the hydrate cages were almost identical in Kaol models. The H_2O molecules on the siloxane surface achieved a lower value of F_3 than those on the hydroxyl surface, which implied that a more optimal tetrahedral structure of H_2O molecules was formed on the siloxane surface. This result was in accordance with the distribution of CH_4 and H_2O molecules on the siloxane surface and suggested that the clathrate-like structure was more easily formed near the siloxane surface.

3.1.2. The arrangement of hydrate cages in Kaol particles

To describe in detail the hydrate cages of the different simulation models, the evolution of the hydrate cages as a function of the simulation time was also investigated (Fig. 3). The snapshot of 5^{12}, $5^{12}6^2$, $5^{12}6^3$, and $5^{12}6^4$ cages in the Kaol model and MH model is illustrated in Fig. 4 and Fig. S2. Hydrate cages appeared and disappeared at the beginning of the simulation. The local CH_4 density was identified as a critical parameter for determining the susceptibility of the solution to the nucleation. For Kaol models, it can be seen that the nucleation of hydrate cages, which were 5^{12} cages, first occurred in the bulk-like solution with a high CH_4 concentration. Cage lifetime increased with the increase of CH_4 concentration, which was consistent with previous studies (Jacobson et al., 2010; Sarupria and Debenedetti, 2012). The 5^{12} cages became dominant in the early stage of CH_4 hydrate growth, and the number of $5^{12}6^2$ cages gradually increased. The formation rate of $5^{12}6^3$ cages increased rapidly first and then slowly with increasing simulation time. The formation of $5^{12}6^4$ cages was slower than the formation of 5^{12} and $5^{12}6^2$ cages, and the latter two types of the cages more rapidly reached a stable number. The CH_4 molecule was too small to be effectively stabilized in the $5^{12}6^4$ cages, whereas the $5^{12}6^3$ cages were metastable and has been observed in other studies during CH_4 hydrate formation (Walsh et al., 2009; He et al., 2016). Thus, an amorphous crystal was finally obtained after the CH_4 hydration in various simulation models. The amorphous crystal included both sI (5^{12} and $5^{12}6^2$) and sII (5^{12} and $5^{12}6^4$) motifs, with sI and sII motifs linked by $5^{12}6^3$ cages. The simulation was dominated by the formation of 5^{12} and $5^{12}6^2$ cages, which indicated that the formation of 5^{12} and $5^{12}6^2$ cages was strongly correlated with CH_4 hydrate formation. Therefore, the formation of sI structures was favored over that of sII structures, which was in accordance with the fact that CH_4 molecules can only form sI structures (Sloan and Koh, 2007). The cage ratio (CR) is defined as the ratio of $5^{12}6^2$ cages to 5^{12} cages, and CR can be used to distinguish the amorphous ($CR \leq 1$) structures and CH_4 hydrate crystal structures ($CR > 1$) (Berendsen and Bolhuis, 2019). It was found that the CR ranged from 0.6 to 1.05 (Fig. 3d), which was significantly lower than that of a real sI hydrate ($CR = 3$); moreover, higher CR values were observed in the Kaol model with siloxane surface contacts than the hydroxyl surface contacts. These results indicate that the Kaol particle with the siloxane surface contacts could best increase the crystallinity of CH_4 hydrate. In general, two nucleation events were observed in Kaol models, with one nucleus forming in the bulk-like solution and the other forming near the siloxane surface of Kaol. The crystal growth of CH_4 hydrate crystal typically tended to be away from the Kaol surface. The accumulation of CH_4 molecules on the siloxane surface appeared to decrease the rate of crystal growth in the bulk-like solution, as this accumulation led to the formation of semi-cage structures (compared to the full cage that formed without the Kaol structure). Therefore, the siloxane surface can serve as a facilitator of crystal growth of CH_4 hydrate near the siloxane surface.

To investigate the arrangement of CH_4 and H_2O molecules in various simulation models during CH_4 hydrate formation, the radial distribution function (RDF, $g(r)$) and coordination number (CN, int($g(r)$)) of C-OW, C-C, and OW-OW of the Kaol models during the different

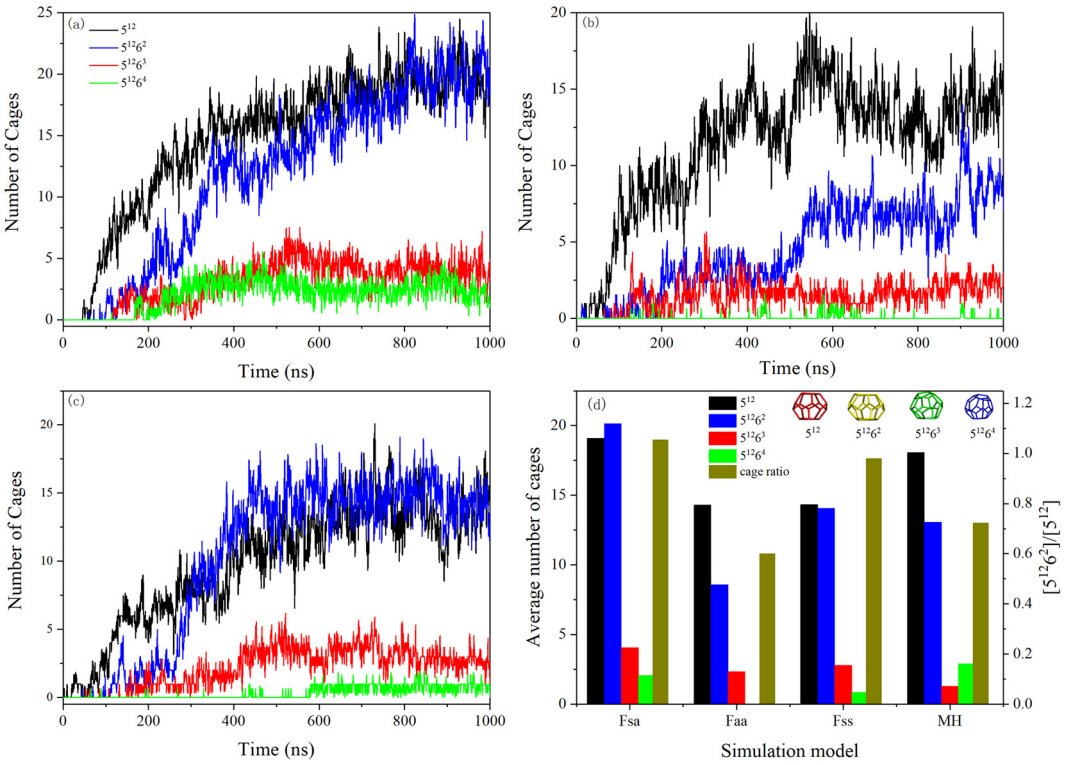

Fig. 3. Evolution of 5^{12}, $5^{12}6^2$, $5^{12}6^3$, and $5^{12}6^4$ cages in Kaol models: (a) Fsa; (b) Faa; (c) Fss; (d) average number of 5^{12}, $5^{12}6^2$, $5^{12}6^3$, and $5^{12}6^4$ cages and cage ratio computed over the last 50 ns of simulation time.

segments of the trajectories were analyzed (Figs. 5 and S3) (where C and OW represent the carbon atom of CH_4 and the oxygen atom of H_2O, respectively) (Allen and Tildesley, 2017). The RDF and CN of C-OW in the MH model are shown in Fig. S4. In all simulation models, the RDF of C-OW showed that its first peak was approximately equal to 0.38 nm, corresponding to the closest distance between CH_4 and H_2O molecules. This result was in good agreement with the neutron diffraction result for CH_4 hydrate (Koh et al., 2000). The RDF of C-OW also captured the growth of hydrate cages as the simulation time increased. According to a previous study (Koh et al., 2000), the CN of H_2O molecules around CH_4 of 21 ± 1 indicated that a CH_4 hydrate was fully formed. In this work, the CN of H_2O molecules around CH_4 was approximately 22.7,

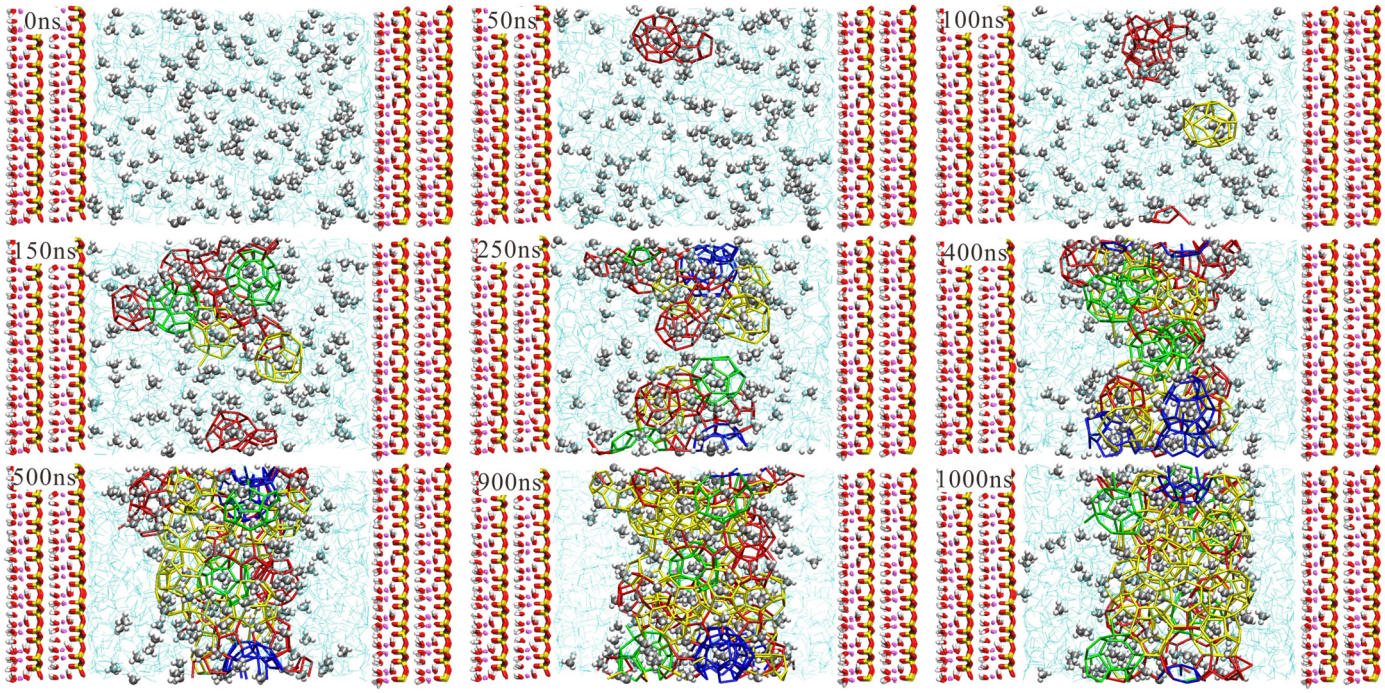

Fig. 4. Snapshots of 5^{12}, $5^{12}6^2$, $5^{12}6^3$, and $5^{12}6^4$ in Fsa model during different simulation times. Hydrate cages are shown with different colors, red for 5^{12}, yellow for $5^{12}6^2$, green for $5^{12}6^3$ and blue for $5^{12}6^4$. (For interpretation of the references to colour in this figure legend, the reader is referred to the web version of this article.)

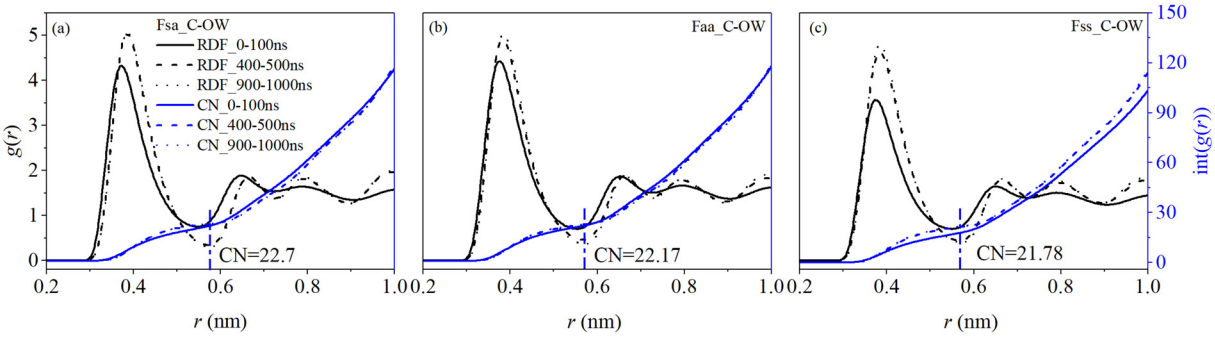

Fig. 5. Radial distribution function and coordination number of C-OW in different simulation models: (a) Fsa, (b) Faa, and (c) Fss.

22.17, 21.78, and 22.52 in Fsa, Faa, Fss, and MH models, respectively, which indicated that a stable CH_4 hydrate structure had indeed been formed. The RDF of C-C and OW-OW were almost identical in all simulation models. From the RDF of C-C (Figs. S3 and S4), the first peak was stronger than the other peaks from 0 to 100 ns, which implied that the system was composed of liquid H_2O and randomly distributed CH_4 molecules. As CH_4 hydrate growth continued as the simulation time increased, the second peak became more pronounced, which demonstrated that both CH_4 and H_2O molecules were arranged in the clathrate-like structures. The strong peak at approximately 0.65 nm was consistent with the distance between CH_4 molecules in the bulk CH_4 hydrate phase (Chialvo et al., 2002). From the RDF of OW-OW (Figs. S3 and S4), it can be seen that the first, second, and third peaks of simulation models were consistent with those for the pure CH_4 hydrate (Chialvo et al., 2002; Geng et al., 2009; Zhang and Pan, 2011). Mean square displacement (MSD) of H_2O and CH_4 in different simulation models was shown in Fig. S5. The MSD profile showed a lower diffusion of H_2O and CH_4 molecules in the Faa model than that in the Fss and Fsa models. This result indicated that the diffusion capacity of H_2O molecules was reduced with the presence of hydroxyl surface in the Kaol particles. Additionally, the different diffusion capacity of H_2O molecules in the MH model and the Kaol model with different surface contacts also indicated that surface properties of Kaol play an important role in the heterogeneous CH_4 hydrate nucleation due to the local arrangement of H_2O molecules.

The silicon-oxygen rings of the siloxane surface of Kaol can also stabilize the CH_4 molecules and promote CH_4 hydrate formation. To show the local structure of CH_4 molecules on the Kaol surface, the RDF among C and OB atoms (oxygen atoms of siloxane surface) in the different segments of the trajectories were also investigated. It can be seen that the first peak appeared at approximately 0.36 nm and that the CN was approximately 0.5 after CH_4 hydrate formed (Fig. 6b), which indicated that a small number of OB atoms were involved in the nucleation of CH_4 hydrate cages. This result was revealed by the distribution of CH_4 molecules, showing that the facility of CH_4 aggregate on the siloxane surface led to the formation of the semi-cage structures.

3.2. Density distribution of CH_4 and H_2O molecules

The average density of CH_4 hydrate was 0.943 g/cm^3 in the MH model, which was in good agreement with previous experimental result (Fig. S6) (Kirchner et al., 2004). The peak of the CH_4 hydrate density corresponded to CH_4 molecules in the large $5^{12}6^2$ cages, and the valleys corresponded to CH_4 molecules in small 5^{12} cages. The density distribution of CH_4 and H_2O molecules in Kaol models was illustrated in Fig. 7. From Fig. 7, two strong peaks for H_2O molecules were observed near the Kaol surface, which implied that a greater adsorption density of H_2O molecules formed on both sides of the Kaol particle. The H_2O density was approximately 2.5 g/cm^3 (hydroxyl surface) and 1.6 g/cm^3 (siloxane surface), and the density decreased in the region farther than 0.3 nm from the Kaol surface. It was observed that CH_4 was more strongly adsorbed to the siloxane surface than to the hydroxyl surface, which implies that the interaction between CH_4 and the hydroxyl surface was weaker than that between CH_4 and the siloxane surface. However, the hydroxyl surface was completely covered by H_2O molecules, and the distribution of CH_4 closely mirrored the distribution of these H_2O molecules in the bulk-like region. The hydrophobic siloxane surface and the interaction between CH_4 and siloxane surface was therefore based on van der Waals forces. The hydroxyl surface seemed to be hydrophilic because it formed strong HB with H_2O molecules (Fig. S7). The van der Waals force was weaker than HB, which may explain why CH_4 cannot penetrate the adsorbed H_2O layer of the hydroxyl surface. Therefore, a greater adsorption density of H_2O molecules was observed on the hydrophilic hydroxyl surface of Kaol.

A careful analysis of the simulation trajectories indicated that the H_2O molecules near the siloxane surface formed the semi-cage structures. Clathrate-like hydrate solids formed adjacent to the semi-cage structures by sharing the latter's polygonal rings (Fig. 8). The resulting irregular semi-cage structure was apparently intermediate between the siloxane surface and the CH_4 hydrate crystal, helping to minimize the structural mismatch between the siloxane surface and CH_4 hydrate phase. Similar structural arrangements have also been observed for CO_2 molecules near a silica surface (Bai et al., 2012). The formation of these

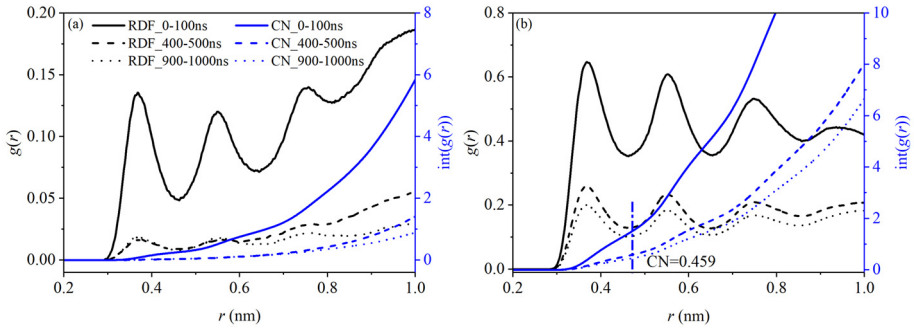

Fig. 6. Radial distribution function and coordination number of C-OB in different simulation models: (a) Fsa; and (b) Fss.

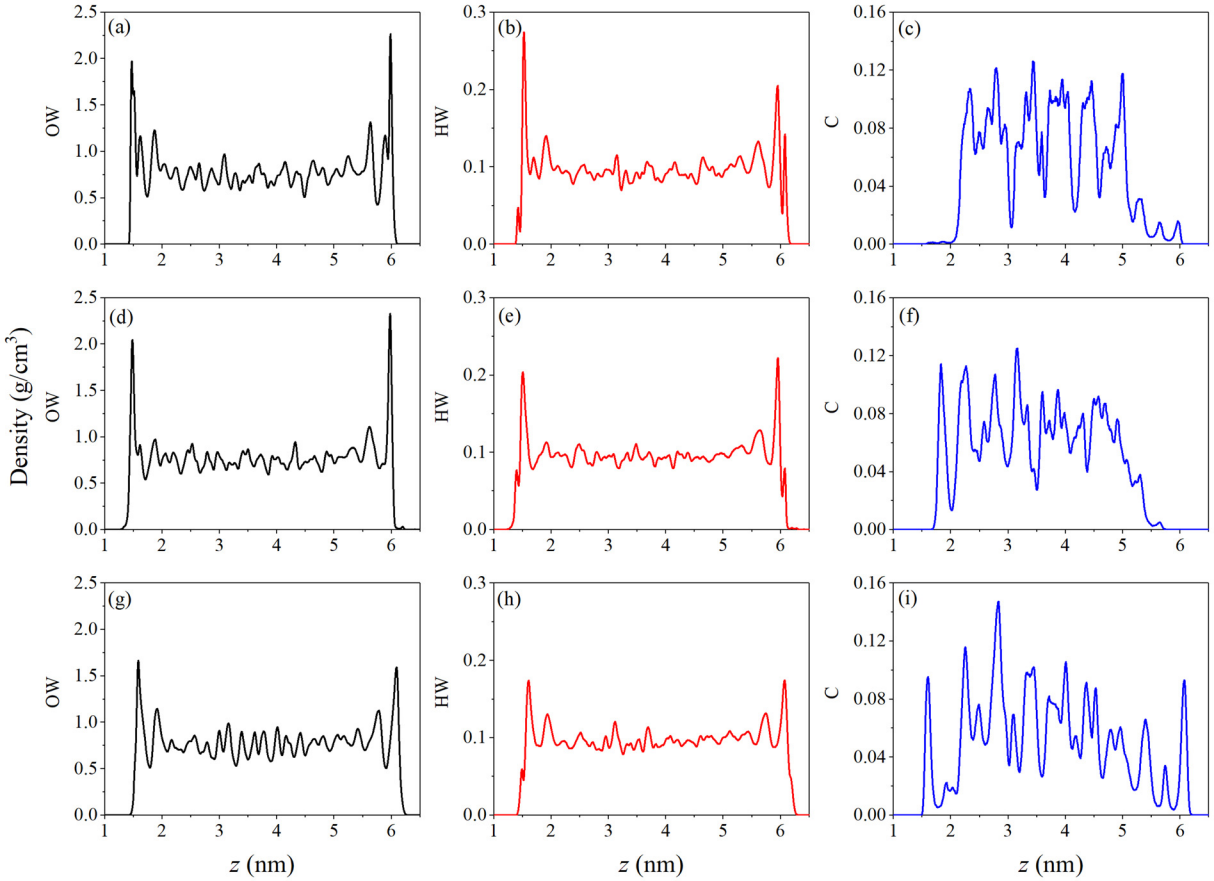

Fig. 7. Density distribution of H_2O oxygen, H_2O hydrogen, and carbon atom of CH_4 in different simulation models: (a–c) Fsa; (d–f) Faa; (g–i) Fss.

semi-cage structures on the siloxane surface of Kaol was due in part to the high local density of CH_4 molecules. CH_4 molecules were favorably adsorbed onto the vacancy of the silicon-oxygen rings of the siloxane surface to form the semi-cage structures (Fig. 9), where the silicon-oxygen rings can serve as a plane of the cage to promote CH_4 hydrate formation. Meanwhile, the semi-cage structure on the Kaol siloxane surface was connected to CH_4 hydrate crystal by the hexagonal face of the $5^{12}6^2$ cages.

3.3. Hydrogen bond structural analysis

To explain why CH_4 molecules cannot break through the adsorbed H_2O layer on the hydroxyl surface, the HB structure was investigated. Fig. S7 showed the RDF of OW-HW, OB-HW, OH-HW, and OW-HO in

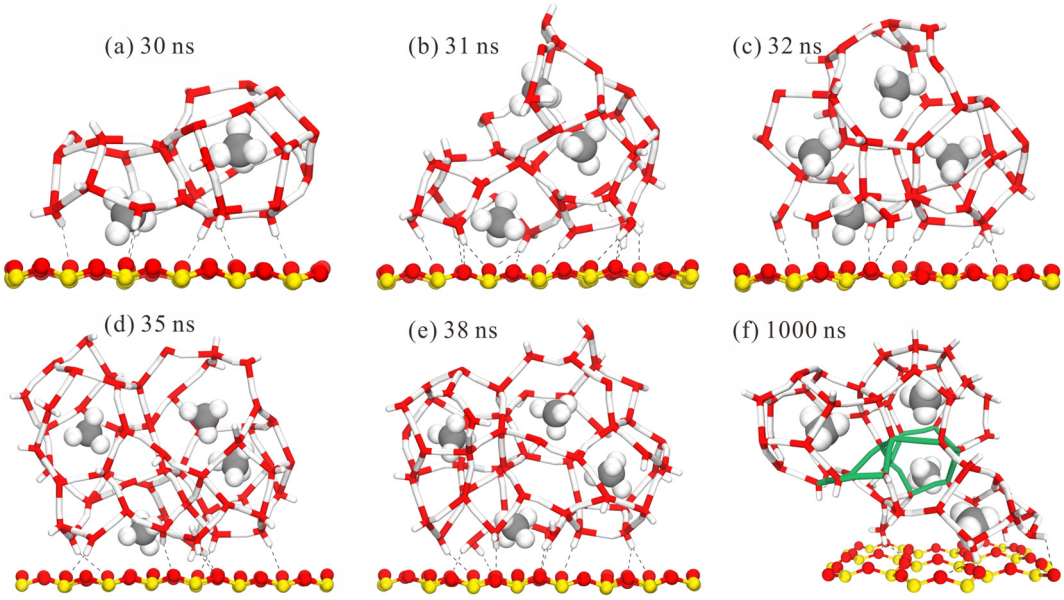

Fig. 8. Structural evolution leading to the formation of the nucleus on the siloxane surface in the Fsa model. Clathrate-like molecules are shown as sticks.

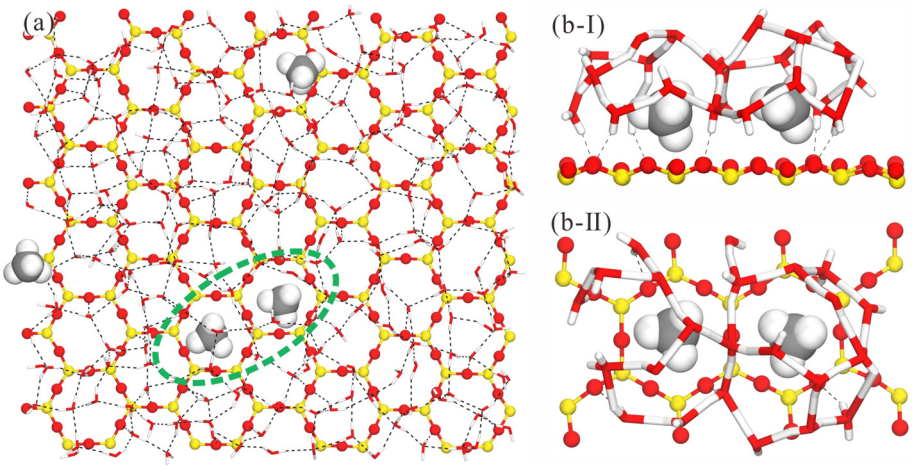

Fig. 9. Snapshot of the distribution of CH4 and H2O on the siloxane surface of the Fsa model (a), side view of the semi-cage structure on the siloxane surface (b-I), the top view of the semi-cage structure on the siloxane surface (b-II).

the Fsa model. It can be seen that the first peak of $g_{OW\text{-}HW}(r)$ was located at 0.183 nm; this represented the HB distance of H_2O molecules in the CH_4 hydrate. The first peak of $g_{OH\text{-}HW}(r)$ and $g_{OW\text{-}HO}(r)$ appeared at approximately 0.175 nm, which indicated that the HB were formed on the hydroxyl surface with H_2O molecules, where these molecules must serve simultaneously as HB donors and acceptors. The intensity of $g_{OW\text{-}HO}(r)$ was also much greater than that of $g_{OH\text{-}HW}(r)$, and this showed that the hydrogen atoms of the hydroxyl surface mainly act as HB donors to form HB with H_2O molecules, which was in agreement with previous work (Zhang et al., 2016). This result was also confirmed from the snapshots of HB structure on the Kaol surface (Fig. S8). The peak of $g_{OB\text{-}HW}(r)$ was at approximately 0.184 nm (Fig. S7), which was the HB distance between OB atoms and H_2O molecules. This HB distance can be used to account for the intensity of the HB structure. Therefore, it was concluded that the HB interaction of the hydroxyl surface was clearly stronger than that of the siloxane surface. In addition, the average number of HB per H_2O molecule contributing to other H_2O molecules was 1.98, 1.92, 1.94, and 1.89 in Fsa, Faa, Fss, and MH models, respectively. The average number of HB per H_2O molecule was 3.87, 3.80, 3.89, and 3.95 in Fsa, Faa, Fss, and MH models, respectively. From comparison with previous studies, these average numbers of HB per H_2O molecules implied that the H_2O molecules were formed in the solid phase (Yan et al., 2016).

The simulation results above demonstrated that the Kaol particles with different surface contacts significantly altered the nucleation pathway and distribution of CH_4 hydrate. The formation of gas hydrate is a continuous process of transformation of H_2O molecules from the liquid phase to a hydrate phase, and gas molecules are trapped in the hydrate cage formed by H_2O molecules (Sloan and Koh, 2007). The CH_4 concentration at the particle interface either increased or remained unchanged, depending on whether the contact surface was hydrophobic or hydrophilic (Nguyen et al., 2017; Guo et al., 2018). In particular, the aggregation of CH_4 on the siloxane surface of the Kaol increased its local concentration. The siloxane surface promoted CH_4 hydrate formation by participating in the formation of a semi-cage structure (Figs. 8 and 9), comprised silicon-oxygen rings of the siloxane surface and some surface H_2O molecules. These semi-cage structures on the siloxane surface might reduce the mismatch between the siloxane surface and CH_4 hydrate crystal by sharing a hexagonal face with $5^{12}6^2$ cages (Fig. 8f). However, the hydroxyl surface preferred to adsorb the H_2O molecules rather than the CH_4 molecules due to the strong HB interaction between hydroxyl surface and H_2O molecules, in contrast to the siloxane surface having a preference for CH_4 molecules, due to its hydrophobicity. As a result, the CH_4 molecules could not break through the adsorption H_2O layer to form semi-cage arrangements on the hydroxyl surface. Meanwhile, the arrangement of H_2O molecules on the siloxane surface tended to increase the local ordering, whereas the H_2O molecules at the hydroxyl surface were less ordered. These data provide a reasonable explanation for the CH_4 hydrate formation in Kaol particles with different surface contacts; that is, the siloxane surface promotes CH_4 hydrate nucleation but the hydroxyl surface fails to promote the nucleation. However, unlike the nucleation and growth mechanism of CH_4 hydrate in Kaol, the formed CH_4 hydrate cages can adsorb dissolved CH_4 molecules on the surface cages of CH_4 hydrate to promote the growth of hydrate cages in pure H_2O. The four types of hydrate cages were gathered together in the MH model (Fig. S2), resulting in the low concentration of CH_4 molecules in the surrounding regions. These findings are in accordance with previous results that showed that the effects of surface hydrophobicity profoundly dominate the nucleation process of CH_4 hydrate (He et al., 2017; Maeda, 2018).

The aggregation behavior of Kaol particles is likely to be dominated by the pH conditions (i.e., low, medium, or high) and ion concentration. One study suggested that the distribution of surface charge densities may affect the surface contacts of Kaol particles at various pH conditions (Gupta and Miller, 2010). Thus, the silica-silica face contact was repulsive in the pH range of 4 to 10 because of the strong electrostatic repulsion, the alumina-alumina face contact was slightly repulsive at a pH of 6 due to a weak electrostatic repulsion and strong van der Waals attraction, whereas the silica-alumina face contact was dominant at pH values below 7.5. Kaol particles are mostly associated with edge-edge and edge-face contacts at a pH of 7. In particular, the silica-alumina face contact promotes edge-face interaction at intermediate pH values (Gupta et al., 2011). However, silica-alumina face and alumina-alumina face contacts are increased at high ion concentration.

The typical pH range of pore water is 7.0 to 8.3 in marine sediment that contains gas hydrate systems (Chatterjee et al., 2011). For instance, the pH range of surface-sediment pore H_2O is 6.9 to 8.3 in the North-South China Sea (Shao et al., 2016) and from 7.4 to 8.6 in the Gulf of Mexico (Cai et al., 2006). Accordingly, the edge-edge, edge-face, and face-face contacts of Kaol particles and particle-H_2O interactions could easily occur in gas hydrate-bearing sediments in these regions. Face-face contact of Kaol particles results in large and thick aggregates (Olphen, 1977), which result in the occurrence of nucleation and distribution of CH_4 hydrate closer to the silica face rather than that of alumina face. The co-existence of edge-face and edge-edge contacts can lead to the formation of three-dimensional networks or a so-called “house of cards” microstructure (Olphen, 1977). Thus, the confining effect of such microstructure may result in the formation of defects in hydrate cages, due to reduced molecular diffusion of CH_4 and H_2O. In addition, the presence of inorganic salts in pore H_2O may cause ionic

adsorption on the Kaol surface. The resulting high concentration of inorganic salts would increase the silica-alumina face and alumina-alumina face contacts and thereby alter the distribution of CH_4 hydrate and the flocculation behavior of Kaol particles that might inhibit or promote CH_4 hydrate formation. Moreover, siloxane and hydroxyl surfaces are the two common types of clay minerals surfaces and are also present in other clay minerals of the marine sediments; for example, montmorillonite, illite, chlorite, and mixed-layer clay minerals contain the siloxane surface, whereas serpentine group minerals possess siloxane and hydroxyl surfaces (Harper et al., 1983; Clennell et al., 1999; Martín-Puertas et al., 2007; Bernárdez et al., 2012). Accordingly, basal surface contacts might be easily formed in the layer stacking of these various clay minerals, leading to similar effects on the nucleation process of CH_4 hydrate.

This study has identified the significant effect that the basal surface contacts of Kaol particles exert on the nucleation and distribution of CH_4 hydrate. This finding is one of the important factor for better understanding the formation mechanism of CH_4 hydrate in any type of clay mineral particles that have siloxane or hydroxyl surface contacts. In particular, the edge surface of clay minerals has a variable (positive or negative) charge that depends strongly on the ambient pH (Luckham and Rossi, 1999; Jozefaciuk and Bowanko, 2002; Bergaya et al., 2013). However, the basal surface of clay minerals has a permanent negative charge that arises from isomorphous substitution in the tetrahedral or octahedral sheet (Bergaya et al., 2013). Consequently, the actual contacts between basal surfaces and edge surfaces are likely to be highly diverse and complex. Therefore, the detailed structural contact behaviors of the edge surfaces of clay mineral particles associated should be considered in further studies on the formation of CH_4 hydrate.

4. Conclusions

Molecular dynamics simulations were performed to investigate CH_4 hydrate formation in Kaol particles with different surface contacts. The results demonstrate that the formation of CH_4 hydrate occurred in the bulk-like region of Kaol particles before the formation of semi-cage occurred near the Kaol surface. The crystallinity of CH_4 hydrate in the Kaol particles with a siloxane surface was superior to that in the bulk hydrate phase. The formation rates of the 5^{12} and $5^{12}6^2$ cages were greater than those of the $5^{12}6^3$ and $5^{12}6^4$ cages, resulting in the sI (5^{12} and $5^{12}6^2$) motif is being favored over the sII (5^{12} and $5^{12}6^4$) motif. CH_4 molecules were easily adsorbed onto the siloxane surface to form a semi-cage arrangement on the siloxane-water interface, which provided further the nucleation sites for CH_4 hydrate formation. However, the disordered structure of H_2O molecules near the hydroxyl surface did not necessarily promote CH_4 hydrate nucleation.

In general, the results suggest that the formation of CH_4 hydrate on the Kaol particles differed greatly from that in the bulk hydrate phase owing to the surface effects of the particles. For example, the H_2O molecules at the hydrophobic siloxane surface adopted a regular tetrahedral arrangement that was conducive to CH_4 hydrate formation. Furthermore, the layered stacking of clay mineral particles should be considered a key factor for developing a better understanding of the formation of CH_4 hydrate in marine sediments.

Declaration of Competing Interest

We declare that we have no known competing financial interests or personal relationships that could have appeared to influence the work reported in this paper.

Acknowledgments

This work was supported by National Special Support for High-Level Personnel and Youth Innovation Promotion Association CAS for the excellent members (2016-81-01), National Natural Science Foundation of China (Grant Nos. 41472044 41272059, and 41602034), This is a contribution (No. IS-2793) from GIGCAS.

Appendix A. Supplementary data

Supplementary data to this article can be found online at https://doi.org/10.1016/j.clay.2020.105439.

References

Özen, İ., Süleyman, Ş., Okyay, G., 2015. Manipulating surface wettability and oil absorbency of diatomite depending on processing and ambient conditions. Appl. Surf. Sci. 332, 22–31.
Abascal, J.L.F., Sanz, E., García-Fernández, R., Vega, C., 2005. A potential model for the study of ices and amorphous water: TIP4P/Ice. J. Chem. Phys. 122, 268–342.
Allen, M.P., Tildesley, D.J., 2017. Computer Simulation of Liquids, 2nd ed. Oxford University Press, Oxford.
Baez, L.A., Clancy, P., 1994. Computer simulation of the crystal growth and dissolution of natural gas hydrates. Ann. N. Y. Acad. Sci. 715, 177–186.
Bai, D., Chen, G., Zhang, X., Wang, W., 2012. Nucleation of the CO_2 hydrate from three-phase contact lines. Langmuir. 28, 7730–7736.
Berendsen, T.A., Bolhuis, P.G., 2019. Unbiased atomistic insight in the competing nucleation mechanisms of methane hydrates. Proc. Natl. Acad. Sci. 116, 19305–19310.
Bergaya, F., Theng, B.K.G., Lagaly, G., 2013. Handbook of Clay Science. Volume 1 Elsevier, Amsterdam Developments of Clay Science.
Bernárdez, P., Prego, R., Giralt, S., Esteve, J., Caetano, M., Parra, S., Francés, G., 2012. Geochemical and mineralogical characterization of surficial sediments from the Northern Rias: Implications for sediment provenance and impact of the source rocks. Mar. Geol. 291-294, 63–72.
Bhattacharjee, G., Choudhary, N., Kumar, A., Chakrabarty, S., Kumar, R., 2016. Effect of the amino acid l-histidine on methane hydrate growth kinetics. J. Nat. Gas Sci. Eng. 35, 1453–1462.
Bish, D.L., 1993. Rietveld refinement of the kaolinite structure at 1.5 K. Clay Clay Miner. 41, 738–744.
Boswell, R., Collett, T.S., Frye, M., Shedd, W., McConnell, D.R., Shelander, D., 2012. Subsurface gas hydrates in the northern Gulf of Mexico. Mar. Pet. Geol. 34, 4–30.
Brigatti, M.F., Galan, E., Theng, B.K.G., 2013. Structure and mineralogy of clay minerals. In Dev. Clay Sci. Elsevier, pp. 21–81.
Cai, W.J., Chen, F., Powell, E.N., Walker, S.E., Parsons-Hubbard, K.M., Staff, G.M., Brett, C.E., 2006. Preferential dissolution of carbonate shells driven by petroleum seep activity in the Gulf of Mexico. Earth Planet. Sci. Lett. 248, 227–243.
Chatterjee, S., Dickens, G.R., Bhatnagar, G., Chapman, W.G., Dugan, B., Snyder, G.T., Hirasaki, G.J., 2011. Pore water sulfate, alkalinity, and carbon isotope profiles in shallow sediment above marine gas hydrate systems: a numerical modeling perspective. J. Geophys. Res. Solid Earth 116.
Chialvo, A.A., Houssa, M., Cummings, P.T., 2002. Molecular Dynamics Study of the Structure and Thermophysical Properties of Model sI Clathrate Hydrates. J. Phys. Chem. B 106, 442–451.
Clennell, M.B., Henry, P., Hovland, M., Booth, J.S., Winters, W.J., Thomas, M., 1999. Formation of Natural Gas Hydrates in Marine Sediments: Gas Hydrate Growth and Stability Conditioned by Host Sediment Properties. Ann. N. Y. Acad. Sci. 912, 887–896.
Cox, S.J., Taylor, D.J., Youngs, T.G., Soper, A.K., Totton, T.S., Chapman, R.G., Michaelides, A., 2018. Formation of methane hydrate in the presence of natural and synthetic nanoparticles. J. Am. Chem. Soc. 140, 3277–3284.
Cygan, R.T., Guggenheim, S., Koster van Groos, A.F., 2004a. Molecular models for the intercalation of methane hydrate complexes in montmorillonite clay. J. Phys. Chem. B 108, 15141–15149.
Cygan, R.T., Liang, J.J., Kalinichev, A.G., 2004b. Molecular models of hydroxide, oxyhydroxide, and clay phases and the development of a general force field. J. Phys. Chem. B 108, 1255–1266.
Darden, T., York, D., Pedersen, L., 1993. Particle mesh Ewald-An N.log (N) method for Ewald sums in large systems. J. Chem. Phys. 98, 10089–10092.
Defever, R.S., Sarupria, S., 2018. Surface chemistry effects on heterogeneous clathrate hydrate nucleation: a molecular dynamics study. J. Chem. Thermodyn. 117, 205–213.
Evans, D.J., Holian, B.L., 1985. The nose-hoover thermostat. J. Chem. Phys. 83, 4069–4074.
Geng, C.Y., Wen, H., Zhou, H., 2009. Molecular simulation of the potential of methane reoccupation during the replacement of methane hydrate by CO_2. J. Phys. Chem. A 113, 5463–5469.
Guggenheim, S., van Groos, A.F.K., 2003. New gas-hydrate phase: synthesis and stability of clay-methane hydrate intercalate. Geology. 31, 653–656.
Guo, Y., Xiao, W., Pu, W., Hu, J., Zhao, J., Zhang, L., 2018. CH_4 nanobubbles on the hydrophobic solid-water interface serving as the nucleation sites of methane hydrate. Langmuir. 34, 10181–10186.
Gupta, V., Miller, J.D., 2010. Surface force measurements at the basal planes of ordered kaolinite particles. J. Colloid Interface Sci. 344, 362–371.
Gupta, V., Hampton, M.A., Stokes, J.R., Nguyen, A.V., Miller, J.D., 2011. Particle interactions in kaolinite suspensions and corresponding aggregate structures. J. Colloid Interface Sci. 359, 95–103.
Harper, G.G., Manley, F.H., Staheli, A.C., 1983. Seismic stratigraphy and clay mineral distribution in shallow-marine siliciclastic deposits, central Mississippi sound, North-

central Gulf of Mexico. Am. Assoc. Pet. Geol. Bull. 67.
He, Z., Gupta, K.M., Linga, P., Jiang, J., 2016. Molecular insights into the crystal nucleation and growth of CH_4 and CO_2 mixed hydrates from microsecond simulations. J. Phys. Chem. C 120, 25225–25326.
He, Z., Linga, P., Jiang, J., 2017. CH_4 Hydrate Formation between Silica and Graphite Surfaces: Insights from Microsecond Molecular Dynamics Simulations. Langmuir. 33, 11956–11967.
Hess, B., Kutzner, C., Van Der Spoel, D., Lindahl, E., 2008. GROMACS 4: algorithms for highly efficient, load-balanced, and scalable molecular simulation. J. Chem. Theory Comput. 4, 435–447.
Jacobson, L.C., Hujo, W., Molinero, V., 2009. Thermodynamic stability and growth of guest-free clathrate hydrates: a low-density crystal phase of water. J. Phys. Chem. B 113, 10298–10307.
Jacobson, L.C., Hujo, W., Molinero, V., 2010. Amorphous precursors in the nucleation of clathrate hydrates. J. Am. Chem. Soc. 132, 11806–11811.
Ji, H., Chen, D., Chen, Z., Wu, G., 2017. Molecular dynamics simulation of methane hydrate formation and dissociation in the clay pores with fatty acids. J. Phys. Chem. C 122, 1318–1325.
Jiménez-Ángeles, F., Firoozabadi, A., 2014. Nucleation of methane hydrates at moderate subcooling by molecular dynamics simulations. J. Phys. Chem. C 118, 11310–11318.
Jiménez-Ángeles, F., Firoozabadi, A., 2015. Enhanced hydrate nucleation near the limit of stability. J. Phys. Chem. C 119, 8798–8804.
Jiménez-Ángeles, F., Firoozabadi, A., 2018. Hydrophobic hydration and the effect of NaCl salt in the adsorption of hydrocarbons and surfactants on clathrate hydrates. ACS Cent. Sci. 4, 820–831.
Johnson, S.B., Russell, A.S., Scales, P.J., 1998. Volume fraction effects in shear rheology and electroacoustic studies of concentrated alumina and kaolin suspensions. Colloids Surf. A Physicochem. Eng. Asp. 141, 119–130.
Johnson, S.B., Franks, G.V., Scales, P.J., Boger, D.V., Healy, T.W., 2000. Surface chemistry-rheology relationships in concentrated mineral suspensions. Int. J. Miner. Process. 58, 267–304.
Jorgensen, W.L., Madura, J.D., Swenson, C.J., 1984. Optimized intermolecular potential functions for liquid hydrocarbons. J. Am. Chem. Soc. 106, 6638–6646.
Jozefaciuk, G., Bowanko, G., 2002. Effect of acid and alkali treatments on surface areas and adsorption energies of selected minerals. Clay Clay Miner. 50, 771–783.
Kim, D., Ahn, Y.H., Kim, S.J., Lee, J.Y., Lee, J., Seo, Y.J., Lee, H., 2015. Gas hydrate in crystalline-swelled clay: the effect of pore dimension on hydrate formation and phase equilibria. J. Phys. Chem. C 119, 22148–22153.
Kirchner, M.T., Boese, R., Billups, W.E., Norman, L.R., 2004. Gas hydrate single-crystal structure analyses. J. Am. Chem. Soc. 126, 9407–9412.
Koh, C.A., Wisbey, R.P., Wu, X., Westacott, R.E., Soper, A.K., 2000. Water ordering around methane during hydrate formation. J. Chem. Phys. 113, 6390–6397.
Kyung, D., Lee, K., Kim, H., Lee, W., 2014. Effect of marine environmental factors on the phase equilibrium of CO_2 hydrate. Int. J. Greenhouse Gas Control. 20, 285–292.
Kyung, D., Lim, H.K., Kim, H., Lee, W., 2015. CO_2 hydrate nucleation kinetics enhanced by an organo-mineral complex formed at the montmorillonite-water interface. Environ. Sci. Technol. 49, 1197–1205.
Lamorena, R.B., Lee, W., 2008. Formation of carbon dioxide hydrate in soil and soil mineral suspensions with electrolytes. Environ. Sci. Technol. 42, 2753–2759.
Lamorena, R.B., Lee, W., 2009. Effect of pH on carbon dioxide hydrate formation in mixed soil mineral suspensions. Environ. Sci. Technol. 43, 5908–5914.
Lamorena, R.B., Kyung, D., Lee, W., 2011. Effect of organic matters on CO_2 hydrate formation in Ulleung Basin sediment suspensions. Environ. Sci. Technol. 45, 6196–6203.
Lee, K.M., Lee, H., Lee, J., Kang, J.M., 2002. CO_2 hydrate behavior in the deep ocean sediments; phase equilibrium, formation kinetics, and solubility. Geophys. Res. Lett. 29, 4–30.
Lee, K., Lee, S.H., Lee, W., 2013. Stochastic nature of carbon dioxide hydrate induction times in Na-montmorillonite and marine sediment suspensions. Int. J. Greenhouse Gas Control. 14, 15–24.
Liang, S., Kusalik, P.G., 2010. Explorations of gas hydrate crystal growth by molecular simulations. Chem. Phys. Lett. 494, 123–133.
Luckham, P.F., Rossi, S., 1999. The colloidal and rheological properties of bentonite suspensions. Adv. Colloid Interf. Sci. 82, 43–92.
Maeda, N., 2018. Interfacial nanobubbles and the memory effect of natural gas hydrates. J. Phys. Chem. C 122, 11399–11406.
Makov, G., Payne, M.C., 1995. Periodic boundary conditions in ab initio calculations. Phys. Rev. B 51, 4014–4022.
Martín-Puertas, C., Mata, M.P., Fernández-Puga, M.C., del Río, V.D., Vázquez, J.T., Somoza, L., 2007. A comparative mineralogical study of gas-related sediments of the Gulf of Cádiz. Geo-Mar. Lett. 27, 223–235.
Martos-Villa, R., Guggenheim, S., Mata, M.P., Sainz-Díaz, C.I., Nieto, F., 2014a. Interaction of methane hydrate complexes with smectites: Experimental results compared to molecular models. Am. Mineral. 99, 401–414.
Martos-Villa, R., Mata, M.P., Sainz-Díaz, C.I., 2014b. Characterization of CO_2 and mixed methane/CO_2 hydrates intercalated in smectites by means of atomistic calculations. J. Mol. Graphics Modell. 49, 80–90.
Moon, C., Hawtin, R.W., Rodger, P.M., 2007. Nucleation and control of clathrate hydrates: insights from simulation. Faraday Discuss. 136, 367–382.
Nguyen, N.N., Nguyen, A.V., Steel, K.M., Dang, L.X., Galib, M., 2017. Interfacial gas enrichment at hydrophobic surfaces and the origin of promotion of gas hydrate formation by hydrophobic solid particles. J. Phys. Chem. C 121, 3830–3840.
Olphen, H.V., 1977. An Introduction to Clay Colloid Chemistry, for Clay Technologists, Geologists, and Soil Scientists, 2nd Edition. .
Park, S.H., Sposito, G., 2003. Do montmorillonite surfaces promote methane hydrate formation? Monte Carlo and molecular dynamics simulations. J. Phys. Chem. B 107, 2281–2290.
Park, T., Kyung, D., Lee, W., 2014. Effect of organic matter on CO_2 hydrate phase equilibrium in phyllosilicate suspensions. Environ. Sci. Technol. 48, 6597–6603.
Parrinello, M., Rahman, A., 1981. Polymorphic transitions in single crystals: a new molecular dynamics method. J. Appl. Phys. 52, 7182–7190.
Rodger, P.M., Forester, T.R., Smith, W., 1996. Simulations of the methane hydrate/methane gas interface near hydrate forming conditions conditions. Fluid Phase Equilib. 116, 326–332.
Sarupria, S., Debenedetti, P.G., 2012. Homogeneous nucleation of methane hydrate in microsecond molecular dynamics simulations. J. Phys. Chem. Lett. 3, 2942–2947.
Schroeder, A., Wiesner, M.G., Liu, Z., 2015. Fluxes of clay minerals in the South China Sea. Earth Planet. Sci. Lett. 430, 30–42.
Seo, Y.J., Seol, J., Yeon, S.H., Koh, D.Y., Cha, M., Kang, S.P., Lee, H., 2009. Structural, mineralogical, and rheological properties of methane hydrates in smectite clays. J. Chem. Eng. Data 54, 1284–1291.
Shao, C., Sui, Y., Tang, D., Legendre, L., 2016. Spatial variability of surface-sediment porewater pH and related water-column characteristics in deep waters of the northern South China Sea. Prog. Oceanogr. 149, 134–144.
Sloan, E.D., 2003. Fundamental principles and applications of natural gas hydrates. Nature. 426, 353–359.
Sloan, E.D., Koh, C.A., 2007. Clathrate Hydrates of Natural Gases. CRC Press, Boca Raton.
Tunega, D., Haberhauer, G., Gerzabek, M.H., Lischka, H., 2002. Theoretical study of adsorption sites on the (001) surfaces of 1: 1 clay minerals. Langmuir. 18, 139–147.
Tunega, D., Gerzabek, M.H., Lischka, H., 2004. Ab initio molecular dynamics study of a monomolecular water layer on octahedral and tetrahedral kaolinite surfaces. J. Phys. Chem. B 108, 5930–5936.
Uchida, T., Takeya, S., Chuvilin, E.M., Ohmura, R., Nagao, J., Yakushev, V.S., Narita, H., 2004. Decomposition of methane hydrates in sand, sandstone, clays, and glass beads. J. Geophys. Res. Solid Earth 109.
Van Gunsteren, W.F., Berendsen, H.J., 1988. A leap-frog algorithm for stochastic dynamics. Mol. Simul. 1, 173–185.
Vatamanu, J., Kusalik, P.G., 2006. Unusual crystalline and polycrystalline structures in methane hydrates. J. Am. Chem. Soc. 128, 15588–15589.
Walsh, M.R., Koh, C.A., Sloan, E.D., Sum, A.K., Wu, D.T., 2009. Microsecond simulations of spontaneous methane hydrate nucleation and growth. Science. 326, 1095–1098.
Walsh, M.R., Beckham, G.T., Koh, C.A., Sloan, E.D., Wu, D.T., Sum, A.K., 2011. Methane hydrate nucleation rates from molecular dynamics simulations: effects of aqueous methane concentration, interfacial curvature, and system size. J. Phys. Chem. C 115, 21241–21248.
Wang, J., Wang, R., Yoon, R.H., Seol, Y., 2015. Use of hydrophobic particles as kinetic promoters for gas hydrate formation. J. Chem. Eng. Data 60, 383–388.
Wei, W., Zhang, J.H., Yu, R.Z., Lin, B.B., Chen, L.Q., Peng, Y., Xiao, H.P., 2018. Review on natural gas hydrate in 2017. Sci. Technol. Rev. 36, 83–90.
Wu, G., Ji, H., Tian, L., Chen, D., 2018. Effects of salt ions on the methane hydrate formation and dissociation in the clay pore water and bulk water. Energy Fuel 32, 12486–12494.
Yan, K.F., Li, X.S., Chen, Z.Y., Xia, Z.M., Xu, C.G., Zhang, Z., 2016. Molecular dynamics simulation of the crystal nucleation and growth behavior of methane hydrate in the presence of the surface and nanopores of porous sediment. Langmuir. 32, 7975–7984.
Yeon, S.H., Seol, J., Koh, D.Y., Seo, Y.J., Park, K.P., Huh, D.G., Lee, H., 2011. Abnormal methane occupancy of natural gas hydrates in deep sea floor sediments. Energy Environ. Sci. 4, 421–424.
Zatsepina, O.Y., Pooladi-Darvish, M., 2011. Storage of CO_2 hydrate in shallow gas reservoirs: pre- and post-injection periods. Greenhouse Gases: Sci. Technol. 1, 223–236.
Żbik, M.S., Frost, R.L., 2009. Micro-structure differences in kaolinite suspensions. J. Colloid Interface Sci. 339, 110–116.
Żbik, M.S., Smart, R.S.C., Morris, G.E., 2008. Kaolinite flocculation structure. J. Colloid Interface Sci. 328, 73–80.
Zhang, J., Pan, Z., 2011. Effect of potential energy on the formation of methane hydrate. J. Pet. Sci. Eng. 76, 148–154.
Zhang, L., Lu, X., Liu, X., Yang, K., Zhou, H., 2016. Surface wettability of basal surfaces of clay minerals: insights from molecular dynamics simulation. Energy Fuel 30, 149–160.